A 26–28 GHz Quadrature-Phase Load-Modulated Balanced Amplifier With Inherent Gain Compression Elimination

Haoyang Jia, *Graduate Student Member, IEEE*, Ruijia Liu, *Member, IEEE*, Lin Qi, *Graduate Student Member, IEEE*, and Anding Zhu, *Fellow, IEEE*

***Abstract*—Load-modulated balanced amplifiers (LMBAs) offer compelling efficiency advantages over broad frequency ranges, but their inherent gain compression in the power back-off (PBO) region poses a significant linearity challenge for modern 5G millimeter-wave applications where digital predistortion (DPD) is difficult to deploy. This article presents a quadrature-phase LMBA (QLMBA) that addresses this limitation through a quadrature-phase control signal injection technique. By establishing a 90° phase offset between the balanced amplifier (BA) and control amplifier (CA), the proposed architecture isolates BA and CA power contributions, suppressing the nonlinear gain compression inherent to conventional LMBA designs. A theoretical analysis demonstrates that, with a properly selected CA to BA drive ratio, gain compression can be fully eliminated. Additionally, a reactive compensation network is integrated into the BA output matching network (OMN) to mitigate the imaginary admittance variation introduced by quadrature load modulation (QLM), improving back-off efficiency. A proof-of-concept 26–28 GHz QLMBA fabricated in a 0.12-μm gallium nitride (GaN) HEMT process achieves saturated output power of 32.3 dBm, drain efficiency of 29.3% at peak and 20.71% at 6-dB PBO at 27 GHz, with less than 1 dB gain compression across the full power range. When driven by 100/400 MHz 5G New Radio (NR) frequency range 2 (FR2) 64 QAM signals, the QLMBA achieves an adjacent channel leakage ratio (ACLR) of −34.2/−30.6 dBc and an error vector magnitude (EVM) of 4.5%/5.5% without DPD, demonstrating its suitability for next-generation millimeter-wave transmitters.**

***Index Terms*—Broadband, linearity, load-modulated balanced amplifier (LMBA), millimeter-wave (mm-Wave), power amplifier (PA), wireless transmitter.**

I. Introduction

TO IMPROVE spectrum efficiency, modern wireless communication systems usually use nonconstant envelope modulation signals with high peak to average power ratio (PAPR), which imposes stringent requirements on efficiency and linearity for RF power amplifiers (PAs) [1]. At millimeter-wave (mm-Wave) frequencies, these demands are particularly challenging: 5G New Radio (NR) frequency range 2 (FR2) deployments require PAs that can handle wide-bandwidth (BW) modulated signals with minimal distortion because it is not practical to use digital predistortion (DPD) in dense phased-array architectures. Achieving intrinsic PA linearity alongside high back-off efficiency therefore remains one of the central design challenges in mm-wave transmitter development.

Received 6 March 2026; revised 14 May 2026; accepted 6 July 2026. This work was supported in part by Taighde Éireann–Research Ireland at CONNECT: the Research Ireland Centre for Future Networks under Grant 13/RC/2077_P2. *(Corresponding author: Ruijia Liu.)*

Haoyang Jia, Lin Qi, and Anding Zhu are with the School of Electrical and Electronic Engineering, University College Dublin, Dublin, D04 V1W8 Ireland (e-mail: haoyang.jia@ucdconnect.ie; lin.qi@ucdconnect.ie; anding.zhu@ucd.ie).

Ruijia Liu is with the School of Electrical and Electronic Engineering, University College Dublin, Dublin, D04 V1W8 Ireland, and also with the Institute of Radio Frequency Engineering and Electronics (IHE), Karlsruhe Institute of Technology (KIT), 76131 Karlsruhe, Germany (e-mail: ruijia.liu@ucd.ie; ruijia.liu@kit.edu).

Digital Object Identifier 10.1109/TMTT.2026.3711938

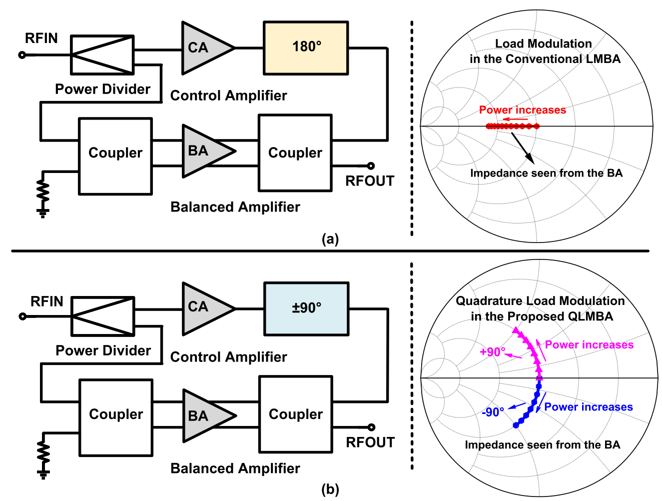

Fig. 1. RF-input LMBA architectures (a) conventional LMBA and (b) proposed QLMBA.

Various PA architectures have been developed to address the efficiency-linearity tradeoff, including outphasing, envelope tracking, and Doherty PAs (DPAs) [2], [3], [4], [5], [6], [7], [8], [9], [10], [11], [12], [13], [14], [15]. Among them, DPA has been widely adopted in wireless base station transmitters due to its high reliability and low complexity [16]. However, conventional DPAs typically rely on $\lambda/4$ transmission lines for load modulation, which imposes limitations on BW, especially for ultra-wideband or multiband signal applications.

Recently, load-modulated balanced amplifier (LMBA) has emerged as a compelling alternative, offering the potential for high back-off efficiency across broad frequency ranges without the BW limitations imposed by Doherty-style quarter-wave networks [17], [18], [19], [20], [21], [22], [23], [24], [25], [26], [27], [28], [29], [30], [31]. LMBA uses a control amplifier (CA) to inject signals into the output of the balanced amplifier (BA) through a coupler. In the RF-input configuration, the BA and CA signals have a constant phase offset of 180°, as illustrated in Fig. 1(a). It can be observed that the BA impedance moves toward lower resistance values along the real axis as the output power increases, thereby improving efficiency in the power back-off (PBO) region.

A modified LMBA architecture, known as the sequential LMBA (SLMBA) or the pseudo-Doherty LMBA (PD-LMBA), utilizes the CA as the main amplifier to amplify the signal up to the PBO point, while the BA works as an auxiliary PA, intervening after the PBO point [32], [33], [34], [35], [36]. The load-modulation in both architectures produces a gain compression beyond the PBO point. This nonlinearity is particularly problematic at mm-wave frequencies where it is difficult to employ highly complex DPD modules to linearize the FR2 wireless communication systems. To mitigate the linearity issue, several approaches have been reported in the literature. [37] presents a method of complex impedance to improve the AM-PM characteristics of LMBA, but did not address the AM-AM characteristics. In [38], a gain flatness enhancement technique is proposed to improve linearity performance through precise coordination of multisection gain profiles with tailored adaptive biasing, which is implemented in a multistage SLMBA. Zhao et al. [39] presents another linearity improvement approach that employs a variable cross-coupled pair (VCCP) combined with an adaptive bias circuit in the CA branch to achieve gain compensation. Nevertheless, the increased design complexity associated with these approaches limits their implementation in high-power gallium nitride (GaN) Monolithic Microwave Integrated Circuit (MMIC).

In this article, we propose a quadrature-phase LMBA (QLMBA) that resolves this linearity limitation through a fundamentally different injection strategy. Instead of injecting the CA signal out-of-phase, the QLMBA injects the control signal through the isolation port of the output coupler with a ±90° phase offset relative to the BA, as shown in Fig. 1(b). This quadrature load modulation (QLM) shifts the BA impedance modulation from the resistive axis to the susceptive axis of the Smith chart, decoupling the BA and CA power contributions and eliminating the nonlinear gain compression inherent to the conventional RF-input LMBA designs. Crucially, this linearity improvement is achieved without additional compensation circuitry or adaptive bias control. To enhance efficiency in the PBO region, a reactive compensation network is introduced at the BA output matching network (OMN) to cancel the imaginary admittance variation imposed by the quadrature injection. A 26–28-GHz RF-input QLMBA was implemented in a 0.12-μm GaN HEMT MMIC process. The measurement results demonstrate excellent linearity and efficiency compared to existing architectures, offering a promising solution for next-generation mm-wave transmitters.

The remainder of this article is organized as follows. Section II presents the operating principle and theoretical analysis of the proposed QLMBA. Section III describes the circuit implementation. Section IV presents the experimental results and comparison with state-of-the-art works, and Section V concludes this article.

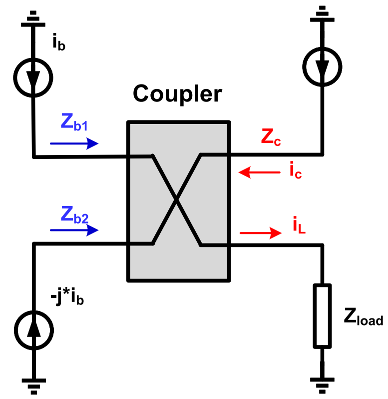

Fig. 2. Simplified block diagram for load modulation analysis.

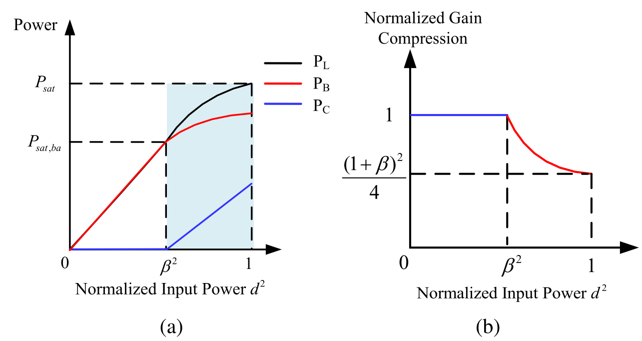

Fig. 3. Linearity of the conventional LMBA architecture. (a) Power performance. (b) Gain compression.

II. Operating Principle of the Proposed Quadrature LMBA

A. Nonlinearity in the Conventional LMBA

To understand the linearity problem in the conventional LMBA and motivate the proposed solution, it is helpful to first establish an analytical framework for load modulation behavior. To facilitate the theoretical derivation, a simplified LMBA architecture with ideal current sources is depicted in Fig. 2. The normalized PBO point is represented by β, d represents the normalized input drive to the overall PA, and Z_o is the coupler characteristic impedance.

In the RF-input LMBA architecture, to achieve the Doherty-like load modulation behavior, Z_b must remain purely resistive and decrease monotonically as the input drive increases. This requires the BA and CA signals to be out-of-phase. Under this condition, Z_{b} can be formulated as [17]

$$Z_{\mathrm{b}} = \left(1 - \frac{\sqrt{2}i_{\mathrm{c}}}{i_{\mathrm{b}}}\right) Z_o \tag{1}$$

where i_{b} and i_{c} are the currents of the BA and CA, respectively.

The resulting load modulation trajectory moves along the real axis of the Smith chart as output power increases, as illustrated in Fig. 1(a). The power delivered to the load under this configuration is given by [18]

$$P_L = \begin{cases} i_b^2 Z_o, & 0 < d < \beta \\ i_b^2 Z_o + \sqrt{2} i_b i_c Z_o + \frac{1}{2} i_c^2 Z_o, & \beta \le d < 1. \end{cases} \quad (2)$$

The source of the linearity problem becomes clear from this expression. Before the PBO point, output power grows quadratically with i_b and hence linearly with input drive. However, beyond the PBO point, when $\beta \le d < 1$, the CA activates and the cross-term $(2)^{1/2} i_b i_c$ introduces an additional nonlinear power increment, and thus the output power is in a nonlinear relationship with the input power, as shown in Fig. 3(a).

Since the BA reaches its maximum drain voltage V_{DB} at $d = \beta$

$$V_{DB} = \left(i_b + \sqrt{2} i_c\right) Z_o = \beta i_b Z_o. \quad (3)$$

Substituting (3) into (2), the gain compression of the conventional LMBA can be derived as

$$GC_{LMBA} = \frac{(1+\beta)^2}{4}. \quad (4)$$

As shown in Fig. 3(b), the LMBA presents a visible gain compression after the PBO point. As the PBO depth increases, the gain compression phenomenon becomes more severe, making the nonlinearity of the PA more prominent.

B. Analysis of the Proposed QLMBA Architecture

To overcome the gain compression in the conventional LMBA, in this work, we propose a new QLMBA architecture. The key idea is to inject the control signal through the isolated port of the coupler with a quadrature phase shift, moving the load modulation from the resistive axis to the susceptive axis of the Smith chart. Under QLM, the CA injection modulates only the imaginary part of the BA admittance, leaving the real part, and hence the BA output power, unchanged. This decoupling between BA and CA power contributions enables linearity improvement.

1) Principle of Operation and Gain Compression Analysis: Since the operating principles of + 90° and −90° are identical while −90° is easier to implement by the transmission line, the remainder of this section considers −90° as a representative case for the theoretical analysis.

As described in [17], when $\theta = -90°$, the power delivered to the load is given as

$$P_{L,-90} = \begin{cases} i_b^2 Z_o, & 0 < d < \beta \\ i_b^2 Z_o + \frac{1}{2} i_c^2 Z_o, & \beta \le d < 1. \end{cases} \quad (5)$$

From this equation, we can see that the output power is only generated from the BA before the PBO point while the increased power after the PBO point depends on the CA power. Fig. 4(a) depicts the power behavior of the proposed QLMBA, where the power of the BA, P_B, increases linearly with the input power before the PBO point and reaches the saturation

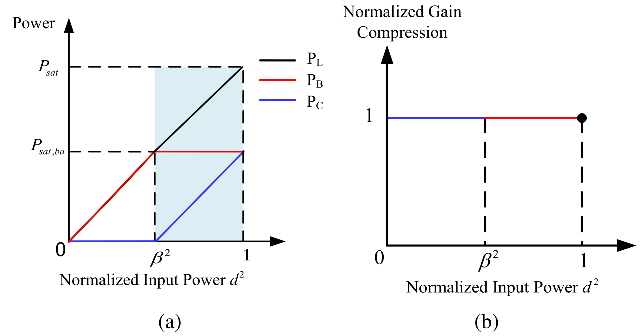

Fig. 4. Linearity of the proposed QLMBA architecture. (a) Power performance. (b) Gain compression.

power $P_{sat,ba}$ at the PBO point. During this power region, the power of the CA, P_C, remains zero, so the output power depends on that of the BA only. After the PBO point, the CA is activated while the power of BA remains constant with the value of $P_{sat,ba}$. If the increased CA power versus the input power is at the same rate of that of the BA power increasing with the input power before PBO, the total power can linearly increase with the input power, which means the nonlinear power increment, that exists in the conventional LMBA, can be eliminated.

Normalizing (5) with respect to the input current and introducing the CA to BA power drive ratio α, the output power can be expressed as

$$P_{L,-90} = \begin{cases} d^2 G_b Z_o, & 0 < d < \beta \\ \beta^2 G_b Z_o + \frac{1}{2}\alpha\left(d^2 - \beta^2\right) G_c Z_o, & \beta \le d < 1 \end{cases} \quad (6)$$

where G_c and G_b are the gain of the CA and BA branch, respectively. The normalized gain compression of the QLMBA can be derived as

$$GC = \frac{\alpha G_c \left(1 - \beta^2\right)}{2 G_b} + \beta^2. \quad (7)$$

To achieve the completely linear QLMBA, the gain compression should be equal to 1, resulting in

$$\alpha = \frac{2 G_b}{G_c}. \quad (8)$$

Supposing the gain of the CA and BA is the same, the normalized gain curves with the PBO level of the proposed QLMBA can be shown in Fig. 4(b). From this figure, it can be noticed that the proposed QLMBA can maintain the consistent linearity and completely eliminate nonlinear gain compression, when α is set to be 2. In other words, when the growth rate of the CA current is $(2)^{1/2}$ times that of a single BA, a linear LMBA can be realized.

2) Power and Efficiency Analysis: Having established the linearization condition, we now examine how the quadrature injection affects overall power and efficiency. The critical distinction from the conventional LMBA is that, under QLM, the CA injection modulates only the imaginary part of the BA admittance.

This article has been accepted for inclusion in a future issue of this journal. Content is final as presented, with the exception of pagination.

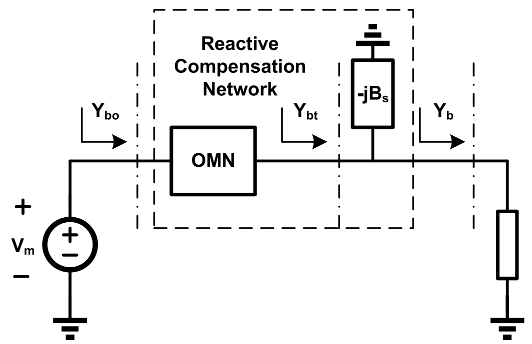

Fig. 5. Simplified diagram of the proposed reactive compensation network.

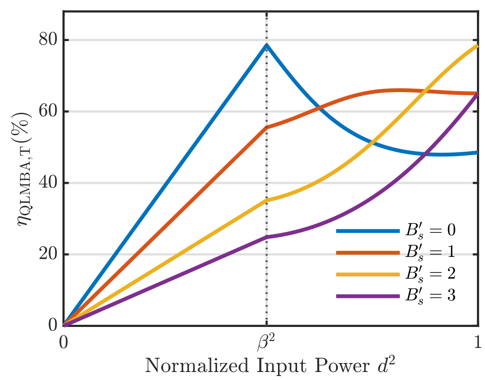

Fig. 6. Efficiency of the proposed QLMBA with the proposed reactive compensation network.

Substituting (3) into (1), the admittance $Y_{b,-90^\circ}$ seen from the BA in QLMBA can be expressed as

$$Y_{b,-90^\circ} = \frac{1}{Z_o} + j\frac{\sqrt{2}i_c}{V_{DB}}. \tag{9}$$

Before the PBO point, the CA is off so that the admittance $Y_{b,-90^\circ}$ reduces to $1/Z_o$, which is the same as that in the conventional LMBA. Beyond the PBO point, the CA is turned on and the imaginary part of $Y_{b,-90^\circ}$ rises along the constant-conductance circle as i_c increases, as shown in Fig. 1(b). Since the real part of the BA admittance remains fixed, the BA output power is constant in the PBO region, with all incremental power supplied by the CA.

However, the growing imaginary admittance also means the BA draws additional reactive current in the PBO region, increasing its DC power consumption. Assuming ideal Class-B operation for both the BA and CA, the DC power consumption of the BA for $d \ge \beta$ is

$$P_{DC,B} = \frac{2}{\pi}\sqrt{\frac{1}{Z_o^2} + \frac{2i_c^2}{V_{DB}^2}} \cdot V_{DB}^2. \tag{10}$$

The overall efficiency of the QLMBA can then be expressed as

$$\eta_{QLMBA} = \begin{cases} \dfrac{\pi}{4}\dfrac{i_b}{V_{DB}} \cdot Z_o, & 0 < d < \beta \\ \dfrac{\pi}{4}\dfrac{2V_{DB}^2 + i_c^2 Z_o^2}{i_c I_C Z_o^2 + 2\sqrt{V_{DB}^4 + 2i_c^2 Z_o^2 V_{DB}^2}}, & \beta \le d < 1 \end{cases} \tag{11}$$

where I_C is the saturated current of the CA. At low power levels, the proposed QLMBA works as the classical class-B that is identical to the conventional LMBA. In the PBO region, due to the imaginary part modulation of Y_b by the QLM, the DC power consumption of the PA increases, resulting in the saturation efficiency not reaching the ideal 78%.

3) Reactive Compensation Network: To compensate the efficiency degradation, we introduce a reactive compensation stub at the BA output, between the transistor and the OMN, which mitigates the imaginary admittance variation introduced by the QLM before it reaches the device, as illustrated in Fig. 5.

If we assume the admittance at the compensation node is

$$Y_{bt} = G_{bt} + jB_{bt}. \tag{12}$$

Considering the introduced shunt stub $-jB_s$, the susceptance in (12) can be expressed as

$$B_{bt} = \frac{\sqrt{2}i_c}{V_{DB}} - \frac{B_s'}{Z_o} \tag{13}$$

where

$$B_s' = B_s \cdot Z_o. \tag{14}$$

Note that the susceptance can be zeroed at one specific amplitude by setting

$$B_s' = \frac{\sqrt{2}i_c Z_o}{V_{DB}} \tag{15}$$

where the imaginary part modulation in the BAs induced by the CA is fully compensated. In this case, (10) can be reformed as

$$P_{DC,bt} = \frac{2}{\pi}\frac{V_{DB}^2}{Z_o} \cdot \sqrt{1 + \left(\frac{\sqrt{2}i_c Z_o}{V_{DB}} - B_s'\right)^2}. \tag{16}$$

Then the efficiency can be given by

$$\eta_{QLMBA,T} = \begin{cases} \dfrac{\pi}{4}\dfrac{i_b Z_o}{V_{DB}\sqrt{1 + B_s'^2}}, & 0 < d < \beta \\ \dfrac{\pi}{4}\dfrac{2V_{DB}^2 + i_c^2 Z_o^2}{i_c I_C Z_o^2 + 2V_{DB}^2\sqrt{1 + \left(\dfrac{\sqrt{2}i_c Z_o}{V_{DB}} - B_s'\right)^2}}, & \beta \le d < 1. \end{cases} \tag{17}$$

The resulting QLMBA efficiency are shown in Fig. 6 for $B_s' = 0, 1, 2, 3$. In the lower-power region, the efficiency increases linearly with input power, and the slope is influenced by the compensation susceptance B_s'. In the high-power region, the CA starts to conduct and the imaginary impedance is introduced into the BA output by QLM, resulting in additional DC consumption. Without compensation, i.e., when $B_s' = 0$, the efficiency continuously decreases. With the "perfect" reactive compensation ($B_s' = 2$), the efficiency increases monotonically with input power and can reach the theoretical maximum at saturation. However, this exact compensation sacrifices efficiency performance in the PBO region. In comparison, slightly insufficient compensation, e.g., $B_s' = 1$, results in

This article has been accepted for inclusion in a future issue of this journal. Content is final as presented, with the exception of pagination.

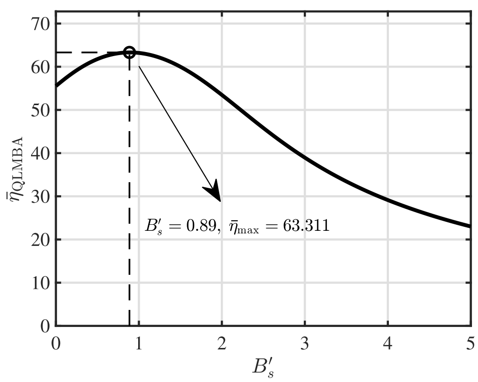

Fig. 7. Average efficiency factor $\bar{\eta}_{\mathrm{QLMBA}}$ over a range of B'_{s}.

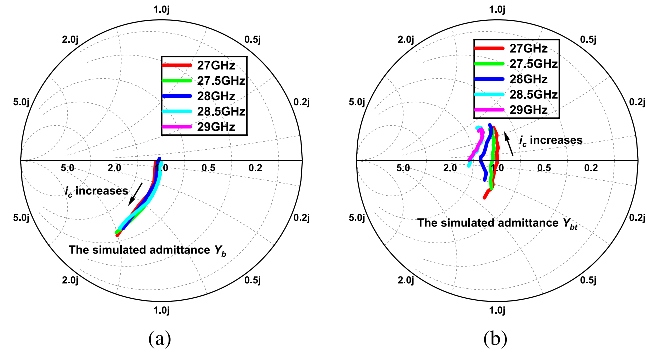

Fig. 8. (a) Simulated admittance Y_{b}. (b) Simulated admittance Y_{bt}.

suboptimal efficiency enhancement across all the high-power levels, indicating how to properly select the value for B'_{s} is critical.

In order to obtain the optimal compensation susceptance B'_{s}, it is necessary to calculate the average efficiency across the entire high power region. For practical modulated signals, the instantaneous power distribution depends on the modulation scheme and the statistics of the signal. In this work, to simplify the derivation, we use the continuous-wave (CW)-based average efficiency factor as a simplified criterion to evaluate the efficiency performance. Since efficiency in the PBO region is the primary concern in QLMBA design, the average efficiency factor is defined as the integral of efficiency over the PBO region, specifically from β^2 to 1, as illustrated in Fig. 6. Then the average efficiency factor can be calculated as

$$\bar{\eta}_{\mathrm{QLMBA}} = \frac{\int_{\beta^2}^{1} \eta_{\mathrm{QLMBA,H}}\left(x_{\mathrm{p}}\right)\, \mathrm{d}x_{\mathrm{p}}}{1-\beta^2} \tag{18}$$

where x_{p} represents the normalized output power, which can be given as

$$x_{\mathrm{p}} = \frac{\beta^2\left(2V_{\mathrm{DB}}^2 + i_{\mathrm{c}}^2 Z_{\mathrm{o}}^2\right)}{2V_{\mathrm{DB}}^2}. \tag{19}$$

To simplify the analysis, $\beta = 1/2$ is assumed to achieve a 6-dB back-off depth. Therefore, the curve of the average efficiency factor over a range of B'_{s} can be plotted as shown in Fig. 7. It can be seen that the maximum average efficiency factor can be obtained when $B'_{\mathrm{s}} = 0.89$ where $\bar{\eta}_{\mathrm{QLMBA}} = 63.3\%$. In comparison, without reactive compensation, i.e., $B'_{\mathrm{s}} = 0$, $\bar{\eta}_{\mathrm{QLMBA}}$ is limited to 55.5%.

As shown in Fig. 5, the matching network can be designed accordingly. At first, B_{s} can be obtained from (14) after the optimal B'_{s} is determined and then the reactive compensation stub TL1 can be designed with the corresponding characteristic impedance and electrical length. Next, OMN is designed to match the compensated admittance Y_{bt} to the required admittance, similar to the traditional PA design. The simulated admittance is shown in Fig. 8, where Y_{bt} is compensated to the x-axis from the modulated imaginary admittance and then matched to Y_{bo} by OMN to acquire the optimal overall efficiency during all the power levels.

III. Implementation of the Proposed QLMBA

A. Architecture Design

To validate the proposed architecture, an RF-input 26–28 GHz QLMBA is designed by using 0.12-μm GaN HEMTs process. The schematic is shown in Fig. 9. The architecture follows directly from the analytical framework developed in Section II: a single RF input is split by a power divider into the BA and CA branches, two two-stage PA units form the BA pair, and a further two-stage amplifier serves as the CA. The output signals are combined through a Lange coupler, which simultaneously performs the 90° hybrid combining function.

Two key design parameters must be carefully established at the architecture level before individual circuit modules are designed. The first is the phase relationship at the combining coupler ports. As derived in Section II-B, the correct current relationships are $i_{b1} = i_b$, $i_{b2} = -j \cdot i_b$, and $i_{ca} = -j \cdot i_c$. To satisfy these conditions, a dedicated transmission line is introduced at the CA output to adjust its phase prior to combining. The second is the CA to BA drive ratio α. From (8), $\alpha = 2$ is required for complete gain compression elimination when the CA and BA have equal gain. This is realized through a power divider with an approximately 2:1 splitting ratio between the BA and CA inputs, ensuring the CA current grows at $(2)^{1/2}$ times the rate of a single BA branch as derived in Section II-B.

B. Circuit Module Design

1) BA and CA: In this work, the BA is biased in class-B to maintain the linearity of the PA units. However, a single stage class-B MMIC PA suffers from low power gain due to its reduced conduction angle. Therefore, a two-stage topology is adopted for the BA to achieve adequate gain. The driver stage uses the same bias voltage as the output stage for simplicity, but with transistors scaled to half the gate periphery to maintain appropriate drive levels without excessive power consumption.

The CA is biased in class-C, which offers two specific advantages. First, the class-C threshold behavior provides a natural on/off switching characteristic that is controlled directly by the gate bias point, activating the CA beyond the PBO point without requiring any external switching,

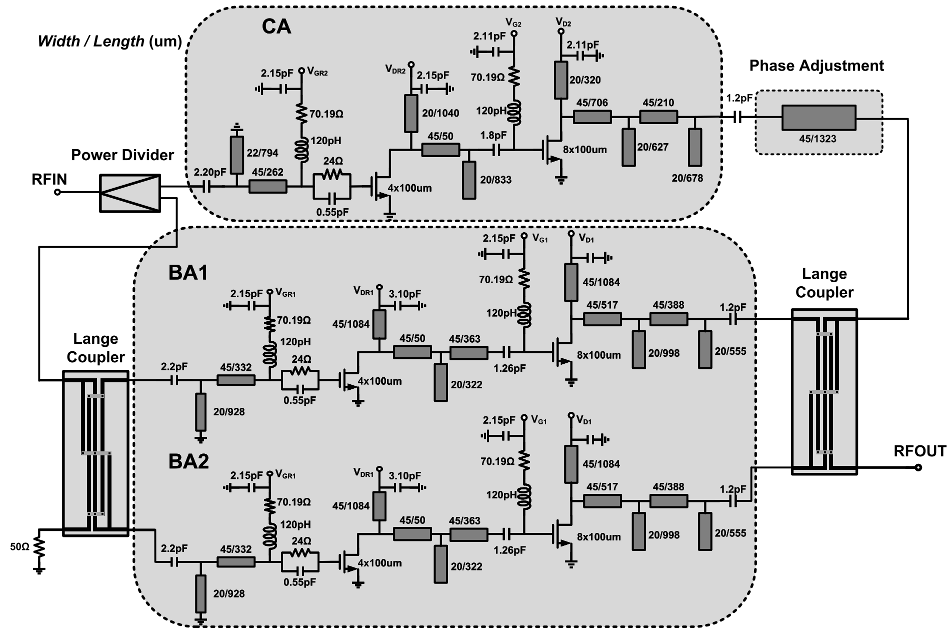

Fig. 9. Schematic of the proposed QLMBA.

simplifying MMIC integration. Second, class-C operation yields higher efficiency than class-B in the high-power region, improving the overall QLMBA efficiency. The same two-stage topology and half-size driver scaling used in the BA are applied to the CA branch for consistency.

The gate bias voltages of the BA and CA transistors are set to −2.3 and −3.2 V respectively to achieve the desired switching behavior between low and high power levels. The supply voltages are set to 15 V for the BA and 28 V for the CA. The higher CA supply extends the high-efficiency range and compensates for the gain reduction introduced by the class-C bias, ensuring that the $\alpha = 2$ drive ratio condition is met over the target frequency range.

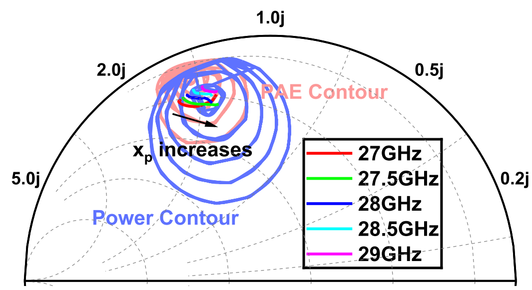

Fig. 10. Normalized simulated admittance Y_{bo} of the proposed QLMBA with the load–pull contours.

2) Lange Coupler: The output coupler is a critical component in the QLMBA, directly determining the quality of load modulation, the achievable BW, and the power combining efficiency. In a MMIC implementation at mm-wave frequencies, the coupler must provide accurate 90° hybrid behavior with low insertion loss over the full 26–28 GHz band. A Lange coupler is selected for this purpose, as its interdigitated multifinger structure generates strong fringing fields at both conductor edges, enabling tight coupling in a compact die area. The designed Lange coupler achieves a 3 dB coupling ratio across the 25–29 GHz band, providing sufficient margin to cover the full target frequency range of the QLMBA.

3) OMN and Reactive Compensation: The OMN design follows the two-step procedure established in Section II-B3. In the first step, the optimal normalized compensation susceptance $B'_s = 0.89$ identified from the average efficiency optimization in Fig. 7 is used to size the reactive compensation stub TL1. The stub characteristic impedance and electrical length are chosen to introduce the required shunt susceptance B_s at the BA output plane, canceling the imaginary admittance variation imposed by the quadrature injection across the operating power range.

In the second step, the OMN transforms the compensated admittance Y_{bt} to the optimal device admittance Y_{bo}. Since the BA and CA operate under different bias conditions, their optimal impedances differ and their matching networks are designed independently. Load–pull simulations are employed to determine the target impedances for peak power and efficiency in each branch. Fig. 10 shows the simulated admittance trajectory Y_{bo} on the Smith chart, confirming that the design point lies at the intersection of the power and power-added efficiency (PAE) contours, achieving the optimal tradeoff between output power and efficiency across all high-power operating levels. The simulated admittance trajectories Y_b and Y_{bt} shown in Fig. 8 further verify that the reactive compensation successfully returns the modulated imaginary admittance to the real axis before the OMN transformation, consistent with the theoretical prediction of Section II-B3.

The fabricated QLMBA occupies a die area of 3.5×2.4 mm^2, and the chip photomicrograph is shown in Fig. 11. On-board decoupling capacitors are used at the bias

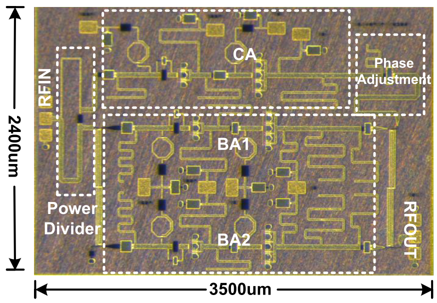

Fig. 11. Chip photograph of the fabricated QLMBA.

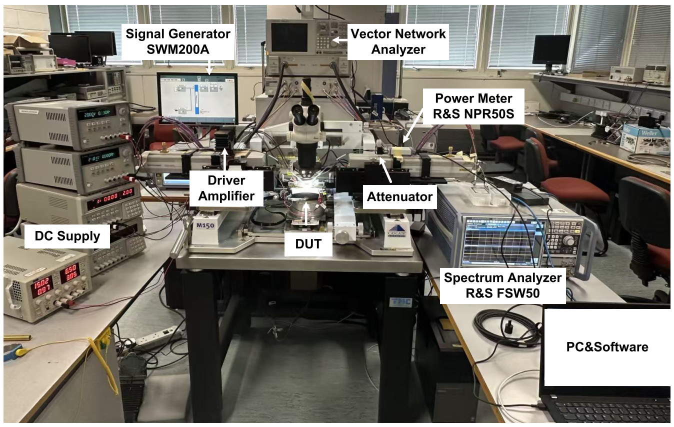

Fig. 12. Photograph of the measurement environment for the implemented QLMBA.

supply pads to suppress source noise and ensure measurement stability.

IV. Measurements Results

To validate the proposed QLMBA architecture, the fabricated chip is wire-bonded to a test PCB with on-board decoupling capacitors at the bias supply pads to suppress source noise and ensure measurement stability. As shown in Fig. 12, the measurement is carried out ON-chip using a probe station with GSG probes employed to connect the input and output. All measured results presented below are de-embedded from cable and connector losses, which are carefully characterized prior to measurement.

A. Small Signal Measurement

Small-signal S-parameter measurements are performed using a vector network analyzer (VNA) E8361A from Agilent. On-wafer short-load-open-thru (SOLT) calibration is applied to move the reference planes from the equipment connectors to the RF probe tips, ensuring accurate de-embedding of the test fixture. The simulated and measured S-parameters are shown in Fig. 13(a). The measured small-signal gain S_{21} reaches 9.2 dB at 27 GHz, with good agreement between simulation and measurement across the full 22–32 GHz sweep range.

To meet the stability requirement, a 1-kΩ resistor was externally added to the gate bias network during the measurements. In practice, the RF-DC isolation is not ideal due to the finite impedance of shunt capacitors and parasitic elements. As a result, the external resistor can couple to the RF signal path and modify the effective impedance seen at the device terminals, leading to the deviations in the measured S_{11} and S_{22} compared to simulation. Nevertheless, the measured results still demonstrate excellent impedance matching across the 26–28 GHz band, validating the effectiveness of the reactive compensation network in maintaining well-matched conditions at the BA output across the operating frequency range.

B. Large Signal Measurement

CW large-signal characterization is performed using a Rohde & Schwarz (R&S) SMW200A signal generator in combination with a highly linear driver amplifier to provide sufficient input drive. Output power is measured using an R&S NRP50S USB thermocouple power sensor with a 20 dB attenuator. The cable and connector losses are carefully characterized first and then de-embedded from the measured data.

The simulated and measured gain and PAE versus output power from 26 to 28 GHz are shown in Fig. 13(b) and (c), respectively. At 27 GHz, the fabricated QLMBA achieves a saturated output power of 32.3 dBm, a peak drain efficiency of 29.3%, and a peak PAE of 24.5%. At 6-dB PBO, drain efficiency of 20.71% and PAE of 16.7% are obtained, representing more than 1.2 times efficiency enhancement over an ideal class-B PA at the same back-off level.

Across this frequency range, the proposed QLMBA maintains consistent performance, with relatively flat gain compression characteristics. The variation in gain across the band is within approximately 2.5 dB, with a slight reduction observed at higher frequencies. Critically, the measured power gain curves in Fig. 13(c) remain flat across the full output power range at all measured frequencies, with a gain compression factor of 0.98, within 1 dB of the small-signal gain up to saturation. This near-unity gain compression factor directly validates the theoretical prediction of Section II-B.

C. Modulated Signal Measurement

The PA operation is also evaluated using a 5G NR frequency range (FR2) 64-QAM signal with 100/400 MHz modulation BW and 9.5/9-dB PAPR. The modulated signal is generated in MATLAB, loaded into an R&S SMW200A vector signal generator, and applied to the PA input. The output signal is captured using an R&S FSW45 vector signal analyzer and post-processed in MATLAB to calculate the adjacent channel leakage ratio (ACLR) and error vector magnitude (EVM). All results are reported without using DPD.

For the 100 MHz signal, the measured results are shown in Fig. 14(a)–(c). The average output power under modulated excitation is 23.2 dBm, which falls within the enhanced linearity PBO region as intended by the QLMBA design. The implemented QLMBA exhibits favorable AM/AM and AM/PM characteristics, achieving an ACLR of −34.2 dBc and an EVM of 4.5%. Both metrics comfortably satisfy the 3GPP NR FR2 requirements of −28 dBc ACLR and 8% EVM without any DPD correction, demonstrating that the intrinsic

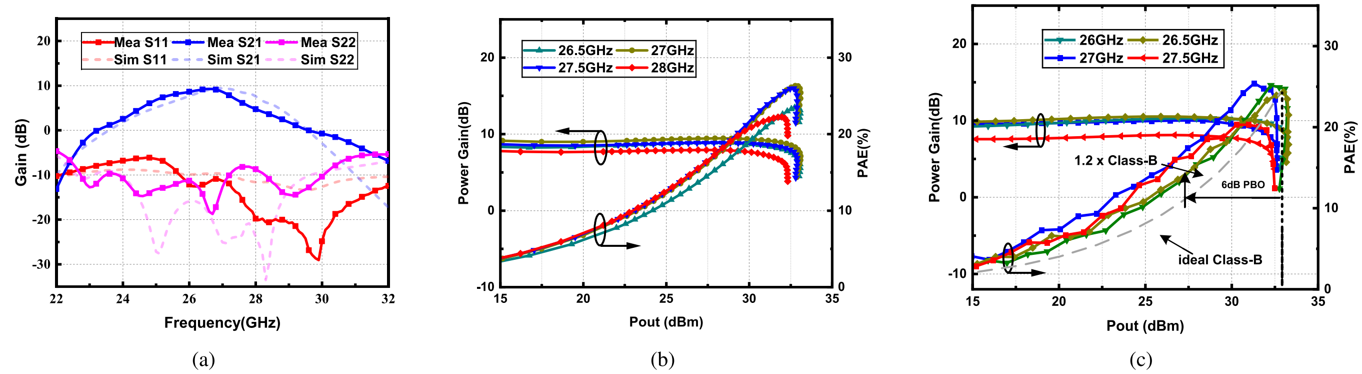

Fig. 13. (a) Simulated and Measured S-parameters, (b) simulated PAE and power gain versus output power, and (c) measured PAE and power gain versus output power.

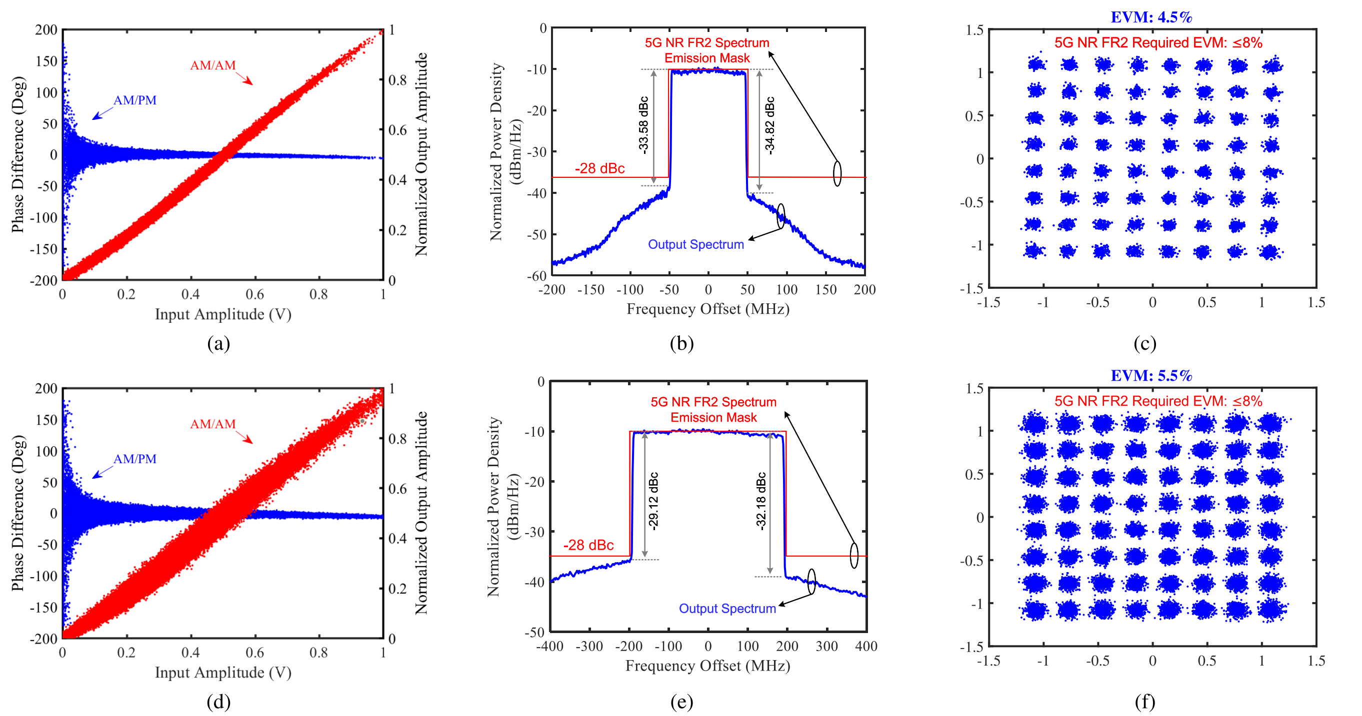

Fig. 14. Modulation signal measurements using 5G NR 64-QAM signals. Results for a 100 MHz signal with 9.5 dB PAPR (a) AM/AM and AM/PM characteristics, (b) output spectrum, and (c) constellation with EVM. Results for a 400 MHz signal with 9.0 dB PAPR (d) AM/AM and AM/PM characteristics, (e) output spectrum, and (f) constellation with EVM.

linearity of the QLMBA architecture is sufficient for standard compliance under 100 MHz 5G NR operation [45].

For the 400 MHz signal, the measured results are shown in Fig. 14(d)–(f). At an average output power of 24 dBm, the QLMBA achieves an ACLR of −30.6 dBc and an EVM of 5.5% with well-behaved AM/AM and AM/PM characteristics, again without DPD. While the wider signal BW predictably results in a modest degradation in both ACLR and EVM relative to the 100 MHz case, due to the increased spectral content falling closer to the channel edges, both metrics remain well within the 3GPP requirements. This result is particularly significant. To the best of the authors' knowledge, no prior published LMBA has demonstrated standard-compliant 400 MHz 5G NR operation without DPD, highlighting the advantage of the proposed quadrature injection mechanism for wideband modulated signal applications.

D. Comparison With State-of-the-Art

Table I summarizes the performance of the fabricated QLMBA in comparison with other state-of-the-art works, including DPAs, conventional LMBAs, and PD-LMBAs.

In terms of linearity, the proposed QLMBA achieves a gain compression factor of 0.98, significantly outperforming all other LMBA entries in the table, which range from 0.55 to 0.66. The only entry with a comparable gain compression factor is the PD-LMBA in [39], which achieves 1.08 but only through an explicit gain flatness enhancement circuit employing VCCPs with adaptive bias control, a technique that substantially increases circuit complexity and poses integration challenges in high-power MMIC processes. The proposed QLMBA achieves superior linearity through the architecture itself, without any additional compensation circuitry.

TABLE I
PERFORMANCE COMPARISON OF OTHER STATE-OF-THE-ART EFFICIENCY ENHANCED PAs

Parameter	[40]TMTT'22	[41]TMTT'17	[42]TMTT'24	[43]ISSCC'26	[39]TMTT'23	[44]TMTT'24	This work	
Process	0.15 μm GaN HEMT	0.15 μm GaAs pHEMT	0.15 μm GaN HEMT	0.15 μm GaN HEMT	65 nm CMOS	0.12 μm GaN HEMT	0.12 μm GaN HEMT	
Arch.	Doherty	Doherty	LMBA	SALMBA	PD-LMBA	LMBA	QLMBA	
Freq. (GHz)	28.5	28.5–31.5	6–18	24–27.5	27	26	26–28	
Supply (V)	20	4	28	26	2	28	28	
Gain (dB)	20	10.5	18.5–24	16–18.3	24.8	7.01	9.27	
P_{sat} (dBm)	34.2	27.8	40.2–42.5	34.3–35.9	22.2	37.6	32.3	
PAE_{peak}(%)	22	38	25-40	28.5–33	30.4	21.3	24.5	
PAE_{6dB}(%)	15	32	15-18.3*	17.1–22.1*	16.5*	17.1	16.7	
DE_{peak}(%)	24.4*	N/A	N/A	29.2–33.5*	30.6*	35.06	29.3	
DE_{6dB}(%)	16.6*	N/A	N/A	17.5–22.4*	16.5*	24.5	20.71	
Modulation	64-QAM @100MHz	64-QAM @30MHz	64-QAM @20MHz	64-QAM @400MHz	64-QAM @100MHz	64-QAM @100MHz	64-QAM @100MHz	64-QAM @400MHz
$EVM^{\#}$ (%)	5	N/A	10	19.3	5	6.4	4.5	5.5
P_{avg} (dBm)	15	19.9	33	26.6	13.2	28	23.2	24
$ACLR^{\#}$ (dBc)	-32	-26	-30	-21.1	-26.3	-34.1	-34.2	-30.6
Gain Compression$^{@}$	0.93*	0.94*	0.625*	0.6*	$1.08^{*\&}$	0.55*	0.98	

$^{@}$The ratio of the gain at the saturated power to the power back-off point. Gain Compression = $Gain_{sat}/Gain_{PBO}$.
$^{\&}$Gain compensation technique is applied. *Value extrapolated from graphs. $^{\#}$Measured results without DPD.

In terms of modulated signal performance, the QLMBA achieves the best ACLR among all entries at 100 MHz (−34.2 dBc) and demonstrates the widest modulation BW with DPD-free standard compliance at 400 MHz. The DPA in [40] achieves comparable EVM at 100 MHz but at a much lower average output power of 15 dBm, and does not report 400 MHz results. The LMBA in [44], which shares the same GaN process as this work, achieves higher saturated output power and peak drain efficiency but exhibits a gain compression factor of only 0.55, underscoring the fundamental linearity limitation of the conventional LMBA architecture that the proposed QLMBA resolves.

In terms of efficiency, the QLMBA achieves competitive back-off performance with 20.71% DE and 16.7% PAE at 6-dB PBO, comparable to the other GaN LMBA entries despite operating at mm-wave frequencies where efficiency is inherently more challenging to maintain. The reactive compensation network introduced in Section II-B plays a key role in preserving this efficiency by mitigating the imaginary admittance variation that would otherwise increase DC power consumption in the PBO region.

Taken together, these results demonstrate that the proposed QLMBA achieves a more favorable linearity-efficiency tradeoff than prior published LMBA architectures, offering a compelling solution for next-generation mm-wave transmitters where DPD complexity must be minimized.

It is worth mentioning that the prototype we made in this work focuses on demonstrating how the linearity of the LMBA can be improved by using the QLMBA architecture. The BW optimization has not been extensively investigated, especially at FR2 band, and thus the prototype was not specifically designed for BW extension. We will work on BW enhancement in our future work.

V. CONCLUSION

This article presented a QLMBA architecture that resolves the intrinsic nonlinearity of conventional LMBA designs, which is particularly useful at mm-wave frequencies where it is difficult to employ highly complex DPD. The central innovation is the use of quadrature-phase signal injection through the coupler isolation port, which shifts the BA impedance modulation from the resistive to the susceptive axis of the Smith chart. This decouples the BA and CA power contributions, eliminating the nonlinear cross-term responsible for gain compression in conventional LMBAs without requiring additional compensation circuitry or adaptive bias control.

A complete theoretical framework was developed to characterize the gain compression, power, and efficiency behavior of the proposed architecture, yielding a closed-form condition on the CA to BA drive ratio α for complete linearization. A reactive compensation network was further introduced to mitigate the imaginary admittance variation imposed by the quadrature injection, recovering efficiency in the PBO region without compromising the linearity benefit.

A proof-of-concept prototype implemented in a 0.12-μm GaN HEMT MMIC process at 26–28 GHz validated the theoretical predictions experimentally. The fabricated QLMBA achieved a saturated output power of 32.3 dBm, a peak drain efficiency of 29.3% and 20.71% drain efficiency at 6-dB PBO, with a gain compression factor of 0.98, the most linear gain response reported among published LMBA architectures to date. Under excitation by 100/400 MHz 5G NR FR2 64-QAM modulated signals, the QLMBA achieved ACLR of −34.2/−30.6 dBc and EVM of 4.5%/5.5% without DPD, satisfying 3GPP NR FR2 requirements at both BWs and demonstrating DPD-free standard compliance at 400 MHz modulation BW for the first time among published LMBA designs.

REFERENCES

[1] S. C. Cripps et al., *RF Power Amplifiers for Wireless Communications*, vol. 250. Norwood, MA, USA: Artech House, 2006.

[2] T. W. Barton and D. J. Perreault, "Theory and implementation of RF-input outphasing power amplification," *IEEE Trans. Microw. Theory Techn.*, vol. 63, no. 12, pp. 4273–4283, Dec. 2015.

[3] T. Barton, "Not just a phase: Outphasing power amplifiers," *IEEE Microw. Mag.*, vol. 17, no. 2, pp. 18–31, Feb. 2016.

[4] R. Wu, Y.-T. Liu, J. Lopez, C. Schecht, Y. Li, and D. Y. C. Lie, "High-efficiency silicon-based envelope-tracking power amplifier design with envelope shaping for broadband wireless applications," *IEEE J. Solid-State Circuits*, vol. 48, no. 9, pp. 2030–2040, Sep. 2013.

[5] S. Hu, F. Wang, and H. Wang, "A 28-/37-/39-GHz linear Doherty power amplifier in silicon for 5G applications," *IEEE J. Solid-State Circuits*, vol. 54, no. 6, pp. 1586–1599, Jun. 2019.

[6] R. Liu, H. Jia, L. Qi, and A. Zhu, "A 24-to-30-GHz GaN MMIC Doherty power amplifier using reduced peaking intrinsic output impedance for bandwidth extension," *IEEE Microw. Wireless Technol. Lett.*, vol. 35, no. 3, pp. 362–365, Mar. 2025.

[7] I. Kim, J. Moon, S. Jee, and B. Kim, "Optimized design of a highly efficient three-stage Doherty PA using gate adaptation," *IEEE Trans. Microw. Theory Techn.*, vol. 58, no. 10, pp. 2562–2574, Oct. 2010.

[8] M. Bao, D. Gustafsson, R. Hou, Z. Ouarch, C. Chang, and K. Andersson, "A 24–28-GHz Doherty power amplifier with 4-W output power and 32% PAE at 6-dB OPBO in 150-nm GaN technology," *IEEE Microw. Wireless Compon. Lett.*, vol. 31, no. 6, pp. 752–755, Jun. 2021.

[9] E. Liu and H. Wang, "A broadband four-way parallel–series Doherty power amplifier for 5G communications," *IEEE J. Solid-State Circuits*, vol. 59, no. 5, pp. 1312–1322, May 2024.

[10] F. Wang and H. Wang, "A high-power broadband multi-primary DAT-based Doherty power amplifier for mm-Wave 5G applications," *IEEE J. Solid-State Circuits*, vol. 56, no. 6, pp. 1668–1681, Jun. 2021.

[11] B. Rabet and J. Buckwalter, "A high-efficiency 28GHz outphasing PA with 23dBm output power using a triaxial balun combiner," in *IEEE Int. Solid-State Circuits Conf. (ISSCC) Dig. Tech. Papers*, Feb. 2018, pp. 174–176.

[12] K. Ning, Y. Fang, N. Hosseinzadeh, and J. F. Buckwalter, "A 30-GHz CMOS SOI outphasing power amplifier with current mode combining for high backoff efficiency and constant envelope operation," *IEEE J. Solid-State Circuits*, vol. 55, no. 5, pp. 1411–1421, May 2020.

[13] J. Lopez et al., "Design of highly efficient wideband RF polar transmitters using the envelope-tracking technique," *IEEE J. Solid-State Circuits*, vol. 44, no. 9, pp. 2276–2294, Sep. 2009.

[14] Y. Li, J. Lopez, P.-H. Wu, W. Hu, R. Wu, and D. Y. C. Lie, "A SiGe envelope-tracking power amplifier with an integrated CMOS envelope modulator for mobile WiMAX/3GPP LTE transmitters," *IEEE Trans. Microw. Theory Techn.*, vol. 59, no. 10, pp. 2525–2536, Oct. 2011.

[15] J. Pang et al., "Broadband GaN MMIC Doherty power amplifier using continuous-mode combining for 5G sub-6 GHz applications," *IEEE J. Solid-State Circuits*, vol. 57, no. 7, pp. 2143–2154, Jul. 2022.

[16] V. Camarchia, M. Pirola, R. Quaglia, S. Jee, Y. Cho, and B. Kim, "The Doherty power amplifier: Review of recent solutions and trends," *IEEE Trans. Microw. Theory Techn.*, vol. 63, no. 2, pp. 559–571, Feb. 2015.

[17] D. J. Shepphard, J. Powell, and S. C. Cripps, "An efficient broadband reconfigurable power amplifier using active load modulation," *IEEE Microw. Wireless Compon. Lett.*, vol. 26, no. 6, pp. 443–445, Jun. 2016.

[18] R. Quaglia and S. Cripps, "A load modulated balanced amplifier for telecom applications," *IEEE Trans. Microw. Theory Techn.*, vol. 66, no. 3, pp. 1328–1338, Mar. 2018.

[19] R. Quaglia, J. Pang, S. C. Cripps, and A. Zhu, "Load-modulated balanced amplifier: From first invention to recent development," *IEEE Microw. Mag.*, vol. 23, no. 12, pp. 60–70, Dec. 2022.

[20] P. H. Pednekar, E. Berry, and T. W. Barton, "RF-input load modulated balanced amplifier with octave bandwidth," *IEEE Trans. Microw. Theory Techn.*, vol. 65, no. 12, pp. 5181–5191, Dec. 2017.

[21] P. H. Pednekar, W. Hallberg, C. Fager, and T. W. Barton, "Analysis and design of a Doherty-like RF-input load modulated balanced amplifier," *IEEE Trans. Microw. Theory Techn.*, vol. 66, no. 12, pp. 5322–5335, Dec. 2018.

[22] Y. Cao, H. Lyu, and K. Chen, "Asymmetrical load modulated balanced amplifier with continuum of modulation ratio and dual-octave bandwidth," *IEEE Trans. Microw. Theory Techn.*, vol. 69, no. 1, pp. 682–696, Jan. 2021.

[23] P. Saad and R. Hou, "Symmetrical load modulated balanced power amplifier with asymmetrical output coupling for load modulation continuum," *IEEE Trans. Microw. Theory Techn.*, vol. 70, no. 4, pp. 2315–2327, Apr. 2022.

[24] D. J. Shepphard, J. Powell, and S. C. Cripps, "A broadband reconfigurable load modulated balanced amplifier (LMBA)," in *IEEE MTT-S Int. Microw. Symp. Dig.*, Jun. 2017, pp. 947–949.

[25] Y. Cao, H. Lyu, and K. Chen, "Continuous-mode hybrid asymmetrical load- modulated balanced amplifier with three-way modulation and multi-band reconfigurability," *IEEE Trans. Circuits Syst. I, Reg. Papers*, vol. 69, no. 3, pp. 1077–1090, Mar. 2022.

[26] L. Chen, H. Liu, J. Hora, J. A. Zhang, K. S. Yeo, and X. Zhu, "A monolithically integrated single-input load-modulated balanced amplifier with enhanced efficiency at power back-off," *IEEE J. Solid-State Circuits*, vol. 56, no. 5, pp. 1553–1564, May 2021.

[27] W. Chen, Y. Wu, S. Li, and W. Wang, "Fully-integrated broadband GaAs MMIC load modulated balanced amplifier for sub-6 GHz applications," *IEEE Trans. Circuits Syst. II, Exp. Briefs*, vol. 70, no. 8, pp. 2834–2838, Aug. 2023.

[28] K. Takenaka, Y. Noguchi, S. Arayashiki, and T. Wada, "Load-modulated balanced amplifier design for handset applications," *IEEE Microw. Wireless Technol. Lett.*, vol. 33, no. 6, pp. 855–858, Jun. 2023.

[29] J. Guo, Y. Cao, and K. Chen, "Linear hybrid asymmetrical load-modulated balanced amplifier with multiband reconfigurability and antenna-VSWR resilience," *IEEE Trans. Microw. Theory Techn.*, vol. 72, no. 9, pp. 5319–5332, Sep. 2024.

[30] P. Gong, J. Guo, N. Bharadwaj Vangipurapu, and K. Chen, "Signal-flow-based analysis and design of pseudo-Doherty load-modulated balanced amplifier toward unlimited RF bandwidth," *IEEE Trans. Microw. Theory Techn.*, vol. 73, no. 1, pp. 206–220, Jan. 2025.

[31] P. Gong, N. Bharadwaj Vangipurapu, J. Guo, and K. Chen, "Doherty-like load-modulated balanced amplifier with decade bandwidth enabled by novel broadband all-port-matched balun," *IEEE Trans. Microw. Theory Techn.*, vol. 74, no. 1, pp. 224–237, Jan. 2026.

[32] C. Chu, J. Pang, R. Darraji, S. K. Dhar, T. Sharma, and A. Zhu, "Broadband sequential load modulated balanced amplifier with extended design space using second harmonic manipulation," *IEEE Trans. Microw. Theory Techn.*, vol. 71, no. 5, pp. 1990–2003, May 2023.

[33] C. Chu et al., "Waveform engineered sequential load modulated balanced amplifier with continuous class-F-1 and class-J operation," *IEEE Trans. Microw. Theory Techn.*, vol. 70, no. 2, pp. 1269–1283, Feb. 2022.

[34] K. Chaudhry, R. Quaglia, and S. Cripps, "A load modulated balanced amplifier with linear gain response and wide high-efficiency output power back-off region," in *Proc. Int. Workshop Integr. Nonlinear Microw. Millim.-Wave Circuits (INMMiC)*, Jul. 2020, pp. 1–3.

[35] J. Pang et al., "Analysis and design of highly efficient wideband RF-input sequential load modulated balanced power amplifier," *IEEE Trans. Microw. Theory Techn.*, vol. 68, no. 5, pp. 1741–1753, May 2020.

[36] Y. Cao and K. Chen, "Pseudo-Doherty load-modulated balanced amplifier with wide bandwidth and extended power back-off range," *IEEE Trans. Microw. Theory Techn.*, vol. 68, no. 7, pp. 3172–3183, Jul. 2020.

[37] K. Vivien, P. E. de Falco, O. Venard, G. Baudoin, P. Pierre-Charles-Félix, and T. Barton, "Load modulated balanced amplifier design method based on complex impedance trajectories," *IEEE J. Microw.*, vol. 2, no. 1, pp. 199–213, Jan. 2022.

[38] J. Chen et al., "A multistage GaAs HBT sequential LMBA with tailored adaptive biasing and gain coordination for linearity enhancement," *IEEE Trans. Microw. Theory Techn.*, vol. 74, no. 2, pp. 1558–1571, Feb. 2026.

[39] C. Zhao et al., "A Ka-band pseudo-Doherty load-modulated balanced amplifier with gain flatness enhancement technique," *IEEE Trans. Microw. Theory Techn.*, vol. 72, no. 6, pp. 3423–3437, Jun. 2024.

[40] A. Piacibello, V. Camarchia, P. Colantonio, and R. Giofrè, "3-way Doherty power amplifiers: Design guidelines and MMIC implementation at 28 GHz," *IEEE Trans. Microw. Theory Techn.*, vol. 71, no. 5, pp. 2016–2028, May 2023.

[41] D. P. Nguyen, J. Curtis, and A.-V. Pham, "A Doherty amplifier with modified load modulation scheme based on load–pull data," *IEEE Trans. Microw. Theory Techn.*, vol. 66, no. 1, pp. 227–236, Jan. 2018.

[42] L. Kang, A. Wu, W. Chen, and X. Chen, "C–Ku-band RF-input load modulated balanced amplifier MMIC utilizing broadband saturation efficiency enhancement technique," *IEEE Trans. Microw. Theory Techn.*, vol. 73, no. 2, pp. 914–925, Feb. 2025.

[43] L. Yu et al., "20.5 A 24-to-27.5GHz self-adaptive load-modulated balanced amplifier for integrated communication, sensing, and power transfer scenarios," in *IEEE Int. Solid-State Circuits Conf. (ISSCC) Dig. Tech. Papers*, Feb. 2026, pp. 348–350.

[44] H. Jia, R. Liu, Q. Wu, and A. Zhu, "A 26-GHz GaN MMIC load-modulated balanced amplifier with miniaturized dual-loop coupler," *IEEE Trans. Microw. Theory Techn.*, vol. 73, no. 1, pp. 530–539, Jan. 2025.

[45] 3rd Generation Partnership Project (3GPP), *3rd Generation Partnership Project (3GPP), Technical Specification Group Radio Access Network; NR; Base Station (BS) Radio Transmission and Reception (Release 15)*, 3GPP, document TS 38.104, Mar. 2019, section 9.

Haoyang Jia (Graduate Student Member, IEEE) received the B.E. and M.E. degrees from South China University of Technology (SCUT), Guangzhou, China, in 2019 and 2022, respectively. He is currently pursuing the Ph.D. degree at the RF and Microwave Research Group, University College Dublin (UCD), Dublin, Ireland.

His current research interests include integrated high-efficiency power amplifier (PA) design and next-generation transmitter/receiver designs.

Mr. Jia was a recipient of the 2025 IEEE MTT-S Graduate Fellowship Award.

Ruijia Liu (Member, IEEE) received the B.E. degree in electronic information science and technology from Southwest Jiaotong University, Chengdu, China, in 2017, and the Ph.D. degree in electromagnetic field and microwave technology from Southeast University, Nanjing, China, in 2022.

From October 2022 to August 2024, he was a Post-Doctoral Research Fellow with the RF and Microwave Research Group, University College Dublin (UCD), Dublin, Ireland. He is currently a tenure-track Assistant Professor (Ad Astra Fellow) with the School of Electrical and Electronic Engineering, UCD. Since June 2026, he has also been a Humboldt Research Fellow with the Institute of Radio Frequency Engineering and Electronics (IHE), Karlsruhe Institute of Technology (KIT), Karlsruhe, Germany. His research interests include advanced GaN MMIC power amplifier and RFIC design for RF, microwave, and millimeter-wave applications.

Lin Qi (Graduate Student Member, IEEE) received the B.E. degree from Nanjing University of Science and Technology, Nanjing, China, in 2020, and the M.E. degree from Southeast University (SEU), Nanjing, in 2023. She is currently pursuing the Ph.D. degree at the RF and Microwave Research Group, University College Dublin (UCD), Dublin, Ireland.

Her current research interests include behavioral modeling and linearization for RF power amplifiers.

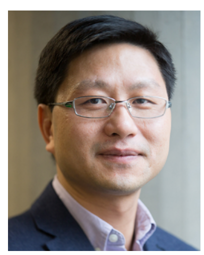

Anding Zhu (Fellow, IEEE) received the Ph.D. degree in electronic engineering from the University College Dublin (UCD), Dublin, Ireland, in 2004.

He is currently a Full Professor with the School of Electrical and Electronic Engineering, UCD. His research interests include high frequency nonlinear system modeling and device characterization techniques, high efficiency power amplifier design, wireless transmitter architectures, digital signal processing, and nonlinear system identification algorithms.

Prof. Zhu is an Elected Member of the IEEE Microwave Theory and Technology Society (MTT-S) Administrative Committee (AdCom) and currently serves as the President of IEEE MTT-S. He was a recipient of the 2021 IEEE MTT-S Microwave Prize. He served as a Track Editor of IEEE TRANSACTIONS ON MICROWAVE THEORY AND TECHNIQUES from 2020 to 2022 and currently an Associate Editor of *IEEE Microwave Magazine*.